CCSP Deliverable D263
Tampere, 2016

Keipi T.

Summary report: Thermo-catalytic decomposition of methane applied to reduce CO_2 emissions in natural gas utilization

ccsp
Carbon Capture and Storage Program

CLIC Innovation Oy
ETELÄRANTA 10
P.O. BOX 10
FI-00131 HELSINKI
FINLAND
www.clicinnovation.fi

CLIC Innovation Oy
Carbon Capture and Storage Program (CCSP)
Deliverable D263

Keipi T.

Summary report: Thermo-catalytic decomposition of methane applied to reduce CO_2 emissions in natural gas utilization

Report Title: Summary report: Thermo-catalytic decomposition of methane applied to reduce CO_2 emissions in natural gas utilization

Key words: Natural gas, hydrogen, pre-combustion carbon capture

Abstract

New and alternative CCS-technologies were innovated at the beginning of the CCSP research program. As a result, the study of thermo-catalytic decomposition of methane (TDM) was started in 2011. TDM is a potential method to enable natural gas utilization with less CO_2-emissions. TDM could be applied to convert the methane in natural gas to solid carbon and gaseous hydrogen. Thus, solid carbon is produced instead of gaseous CO_2. The product carbon from TDM could be easier to storage than the gaseous CO_2, or it may even be a marketable product.

TDM reseach was conducted at the Tampere University of Technology in co-operation with the following partners: Fortum, Gasum, Neste, Helen, ÅF-Consult and VTT Technical Research Centre of Finland. The TDM research results published in 2011–2016 at the Tampere University of Technology are separately listed in references. This report is a summary of the final and unpublished results of the TDM studies.

Tampere, September 2016

Table of contents

1 Introduction

The International Energy Agency (IEA) has predicted that the annual hydrogen demand will increase from the current 7 EJ to 22 EJ in 2050 (IEA, 2015). The main part of the growth is due to the predicted increase in the number of fuel cell vehicles. Currently, the most important process for hydrogen production is the steam methane reforming, which is a significant source of CO_2 emissions. Alternative technologies are required in order to reduce the CO_2 emissions in hydrogen production.

Thermo-catalytic decomposition of methane (TDM) is a reaction where methane converts into gaseous hydrogen and solid carbon. In practice, traces of higher hydrocarbons may also be found among the products. The reaction equation of methane decomposition, which is also known as methane decarburation or (direct) methane cracking, is shown in Eq. 1. (Muradov, 1998).

$$CH_4(g) \rightarrow C(s) + 2H_2(g) \qquad \Delta H_r^0 = +76 \frac{kJ}{mol} \qquad (1)$$

The methane conversion and the properties of the product carbon depend on the reaction conditions, e.g., temperature and reaction time, and on the properties of possibly applied catalyst. Thus far the experimental research on TDM presented in the literature has focused both on thermal and catalytic reactions. The methane decomposition reaction mechanism, the applied catalysts, the properties of the product carbon, several different experimental setups, and possible heating sources for a full-scale application have been extensively summarized in reviews (Amin et al., 2011; Abbas and Daud, 2010; Li et al., 2011; Ashik et al., 2015). Furthermore, the effect of the reaction parameters in TDM on the process design and utilization possibilities of the product carbon has been presented recently in Keipi et al. (2016b)

Already in 1998, Muradov (1998) presented a conceptual idea to apply methane decomposition to natural gas for the on-site production of a gas blend containing hydrogen and methane. A techno-economic analysis of a commercial-scale application for methane decomposition has been conducted previously (Keipi et al., 2016a). In that study, the value of the product carbon was found to be the most important factor affecting the economic feasibility of the entire process. Triphob et al. (2012) have come previously to the same conclusion. Therefore, it is essential to study the properties and quality of the product carbon that originates from the methane decomposition process.

Evaluating the utilization possibilities of the TDM product carbon can be divided into the following steps: (i) the effect of the reaction conditions in methane decomposition on the morphology of the product carbon, (ii) the effect of the morphology on the physical and chemical properties of the product carbon, (iii) the effect of the carbon properties on the utilization possibilities of the product carbon. The first part was studied most recently at the Tampere University of Technology, and the results are presented here.

Moreover, the most important properties of the product carbon related to its utilization possibilities are introduced briefly.

2 Carbon from methane decomposition

As summarized in (Keipi et al. 2016b), the structure of the product carbon that originates from methane decomposition depends on the reaction temperature and catalysts. According to the literature analysis of Keipi et al., the non-catalytic or carbon-catalyzed TDM reaction produces carbon black or graphite-like carbon. In contrast, TDM with metal catalysts produces filamentous carbon, such as carbon nanotubes and nanofibers depending on the catalyst metal. The structure and quality of the product carbon affect the utilization possibilities of the carbon.

2.1 Carbon from non-catalytic TDM

The Encyclopedia of Chemical Technology (Kirk-Othmer, 2007) defines carbon black as a generic name for products which mainly consist of elemental carbon and have an extremely fine particle size. Furthermore, thermal black is defined as a type of carbon black that has larger particle size and is produced by the thermal decomposition of gaseous hydrocarbons, for example, methane. The thermal black process, which uses natural gas as a feedstock, was introduced in the 1920s, but later it was replaced in carbon black production with an oil-furnace process that employs heavy fuel oil as a feedstock (Kirk-Othmer, 2007). The oil-furnace process is still the most widely applied process to produce carbon black (Kirk-Othmer, 2007). The main application for carbon black is a filler in rubber compounds, where it improves the physical properties of the material (Forest, 2001).

Lahaye and Prado (1974) have stated that carbon from the decomposition of gaseous hydrocarbons comes in two different forms. First, pyrolytic carbon forms on the wall of the reactor in the form of small plates with a shape and size determined by the surface that collects the particles. Second, carbon black is also formed in a gaseous phase inside the reactor.

Generally, the formation of carbon black is divided into the following phases: the formation of carbon black precursors from the hydrocarbon molecules at the gas phase, nucleation of the precursors, aggregate formation, surface growth on particles or aggregates, agglomeration due to the collision of the aggregates, and finally the reactions of the carbon black surface with the gas phase (Kirk-Othmer, 2007). The main part of the carbon black mass is produced by surface growth rather than through the formation of new carbon black particles (Heinrich and Klüppel, 2001). The surface growth, which occurs after the formation of aggregates, causes the aggregates to be the smallest existing entity in carbon black (Heinrich and Klüppel, 2001). Thus, aggregates can be separated into particles only by fracturing.

Since the main application for carbon black is rubber products, its properties are generally regarded from that perspective. When the utilization possibilities of the carbon

black are considered, particle size is one of the most important parameters (Kirk-Othmer, 2007). This is because the particle size greatly affects the specific surface area of carbon black, and therefore determines the area where the carbon black can further interface with other compounds. According to (Kirk-Othmer, 2007), increasing the temperature during carbon black formation increases the surface area of carbon black. The specific surface area can be determined from the particle size measurements by using a transmission electron microscope (TEM) or directly with the following standardized methods: nitrogen adsorption, iodine adsorption, and the adsorption of cetyltrimethylammonium bromide (Kirk-Othmer, 2007). Furthermore, the smaller particle size of carbon black indicates better reinforcing properties and abrasion resistance (Speight, 2015).

When considering the everyday use, the carbon black structure, which generally refers to the morphology of the aggregates, is also an important parameter (Kirk-Othmer, 2007). The aggregate size and shape, and the distribution of these factors affect the ability of carbon black to perform as a reinforcing agent or as a pigment (Kirk-Othmer, 2007). In addition to the particle size and structure, the surface activity is also an important parameter affecting the utilization of carbon black (Kirk-Othmer, 2007).

2.2 Carbon from TDM with metal catalysts

Filamentous carbon, also referred to as carbon nanofibers, is produced by the catalytic decomposition of gaseous carbon compounds over metal particles such as iron, cobalt and nickel at temperatures ranging between 400 °C and 1000 °C (Fitzer et al., 1995; Baker, 2001). The production of carbon filaments was developed in the 1950s and the first electron micrographs of the carbon filaments were presented already back then (Harris, 2009). The advances made since on the material characterization have enabled more detailed research of carbon filaments. Recently, the research of carbon filaments has focused on the one hand to prevent the formation of carbon on the catalyst surface, because it deactivates the catalyst, and on the other hand, to produce highly valuable carbon materials, such as carbon nanotubes and carbon nanofibers (Harris, 2009).

The diameter of a carbon filament typically varies from several to a few hundred nanometers (Rodriguez, 1993; Morita et al., 2002), and the diameter is found to be equal with the diameter of the catalyst particle (Rodriguez, 1993; Rodriguez et al., 1995; Poveda and Gupta, 2016). The formation of the carbon filaments follows a three-step-process (Baker, 2001; Rodriguez et al., 1995). First, hydrocarbon decomposes on the catalyst's surface. Second, carbon dissolutes and diffuses through the metal particle. Finally, carbon precipitates to graphite platelets that stack on top of each other forming the nanofiber structure. Furthermore, the carbon diffusion through the catalyst particle is generally considered to be the rate-determining step in the growth process. The presence of hydrogen is also known to enhance the diffusion of carbon in the metal particle (Baker, 2001).

The structure of the carbon filament depends on how the graphite layers are oriented in the filament (Li et al., 2011; Rodriguez et al., 1995). Li et al. (2011) have chosen α, the angle between the graphene layers, to classify the carbon filaments. The platelet filaments have an α value close to 180°, the herringbone or fish-bone structure have an α value between 30 and 150°, and the tubular or parallel filaments have an α value close to 0° (Li et al., 2011). According to (Poveda and Gupta, 2016), faceted catalyst particles produce filaments with a herringbone or a platelet structure and spherical catalyst particles produce a tubular structure. Moreover, the platelet spacing in a filament can be equal with the graphene thickness, 0.335 nm (Rodriguez et al., 1995; Burchell, 2012). Furthermore, the carbon filaments can have a straight or a spiral form. According to (Baker, 2001), the spiral form results from the presence of sulfur or phosphorus that cause asymmetric formation in the carbon filament.

As illustrated in (Li et al., 2011), catalytically induced carbon growth can have two growth mechanisms: base and tip growth. According to (Li et al., 2011), the occurring growth mechanism depends on the metal-support interaction. When the interaction between the metal and support is strong, the metal particles stay on the catalyst's surface and the carbon filaments grow on a metal particle (base growth). With a weaker interaction, the metal particle detaches from the catalyst's surface and moves to the tip of the formed carbon filament (tip growth). The former mechanism has been reported to destroy the catalyst (Li et al., 2011; Frusteri et al., 2012).

The practical application areas for carbon nanofibers are applications in electronics, such as in capacitors and batteries used for energy storage, for composite materials, gas storage by adsorption and as catalyst support material (De Jong and Geus, 2000). In addition to presenting the application areas, De Jong and Geus have specified which properties are the most important in each application. In electronics and in composite materials the electrical properties, such as conductivity and capacitance, are important. When regarding the gas storage applications, higher density is favorable as that indicates larger surface area per volume unit. Furthermore in the gas storage applications, the porosity and pore size distribution in an agglomerate of carbon nanofibers are important properties. The mechanical properties of a single carbon nanofiber, such as elastic properties and tensile strength, are important when the material is applied for catalyst support, especially in liquid-phase catalysis.

3 Experimental research

Experimental studies of TDM without a catalyst (Rajamäki, 2014) and with metal catalysts (Keipi, 2014) have been conducted and reported at the Tampere University of Technology previously. As a follow-up work, the structure and morphology of the product carbon from these studies were analyzed. The selected carbon samples were produced by TDM without a catalyst at the temperature of 800-1200 °C and with a nickel catalyst at temperatures 500 °C, 550 °C and 700 °C. Dr. Mari Honkanen from the Department of Materials Science at the Tampere University of technology is acknowledged for conducting the material characterization analyses.

3.1 Summary of the previously conducted experiments

The experimental studies of TDM without a catalyst are extensively reported in (Rajamäki, 2014). The experimental conditions at the TDM experiments are shortly summarized here. The electrically heated tube reactor (ID 25 mm and length 1000 mm) made of mullite ($3Al_2O_3 \cdot 2SiO_2$) was pre-heated to 800 °C. During the reactor heating and quenching, a constant nitrogen (99.95%) flow of 0.050 dm^3/min was run through the reactor to ensure inert conditions. The methane decomposition experiments were conducted with a continuous methane volume flow of 0.500 dm^3/min.

In each experimental run, the temperature was increased stepwise by 25 °C at a time, and in each step the measured values were recorded after the methane decomposition was stabilized. The product gas composition was examined with a Fourier transform infrared spectroscopy (FTIR) analyzer. Based on these measurements, the methane conversion at each temperature step was calculated (Fig. 1). Five separate runs with these experimental conditions were conducted and the maximum temperatures achieved each time are also marked in Fig. 1.

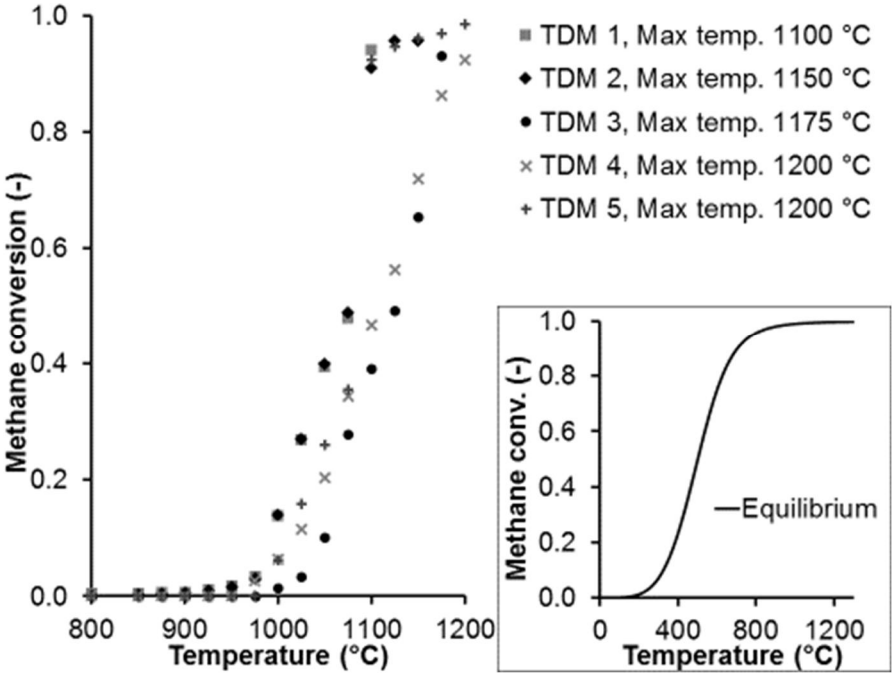

Figure 1. *The measured methane conversion in the TDM experiments as a function of reactor temperature. The insert presents the TDM reaction equilibrium.*

The experimental study of catalytic decomposition of methane (CDM) have been reported previously in Keipi (2014). The experimental arrangement is shortly summarized here. The CDM experiments were conducted at three constant temperatures, i.e., 500 °C, 550 °C, and 700 °C. In these experiments, the reactor functioned as a batch reactor and at the beginning of each CDM experiment a certain number of catalyst

pellets was placed inside the reactor (as presented in the legend in Fig. 2). The applied catalyst in CDM experiments was a commercial nickel catalyst with a thermally durable carrier in the form of a shaped pellet.

When the target temperature was achieved in the hottest section of the reactor, the nitrogen flow was turned off, and the methane flow of 0.150 dm^3/min was turned on. The measurements were ended when no methane decomposition reaction occurred anymore, or the methane conversion remained constant for several hours. The reactor and gas analyzer were the same as in TDM experiments. Four experimental runs were conducted and the methane conversion as a function of reaction time is shown in Fig. 2.

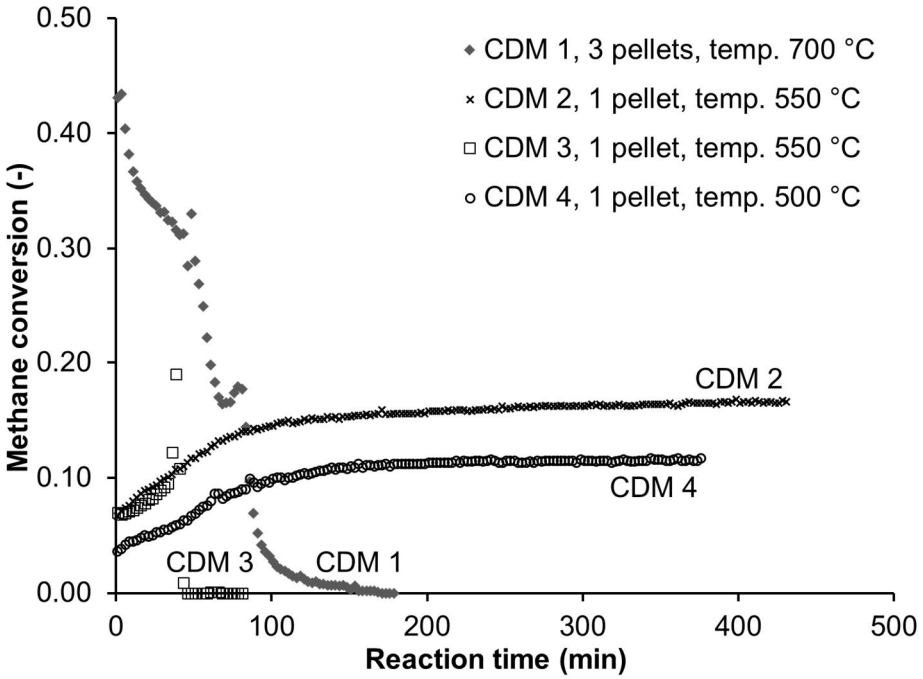

Figure 2. *The measured methane conversion in CDM experiments as a function of reaction time.*

3.2 Analysis methods of the product carbon

The morphology of the selected product carbons was analyzed at the Department of Materials Science at the Tampere University of Technology. The selected product carbons were analyzed by a scanning electron microscope (SEM, Zeiss, ULTRAplus) and a transmission electron microscope (TEM, Jeol, JEM-2010) equipped with an energy dispersive spectrometer (EDS, Thermo Scientific, Noran Vantage with Si(Li) detector). For the SEM analyses the product carbon was attached on the aluminum stub with carbon glue. The samples for TEM analyses were prepared by crushing the product carbon slightly between laboratory glass slides, mixing the powder to ethanol, and applying a drop of powder dispersion onto the copper grid with a holey carbon film.

X-ray diffraction (XRD, PANanalytical, Empyrean Multipurpose Diffractometer with Cu Kα X-ray source (λ=0.15418 nm) and PIXcel^{3D} detector) analyses were also conducted

for selected product carbons. The X-ray diffraction phases were identified by using the database (PDF-4+ 2014) from International Centre for Diffraction Data (ICDD). For powder XRD analyses, the product carbon did not require any special sample preparation.

3.3 Results

3.3.1 XRD analyses

The product carbon from runs CDM 2 and TDM 2 was chosen to further analysis with the help of an XRD analyzer. X-ray diffraction is a method used to determinate the crystallinity of a material. According to these analyses (Fig. 3) the product carbon from both TDM 2 and CDM 2 has a crystalline graphitic structure. Moreover, peaks of the nickel catalyst are also present in the XRD pattern of the CDM 2, which is visible in Fig. 3.

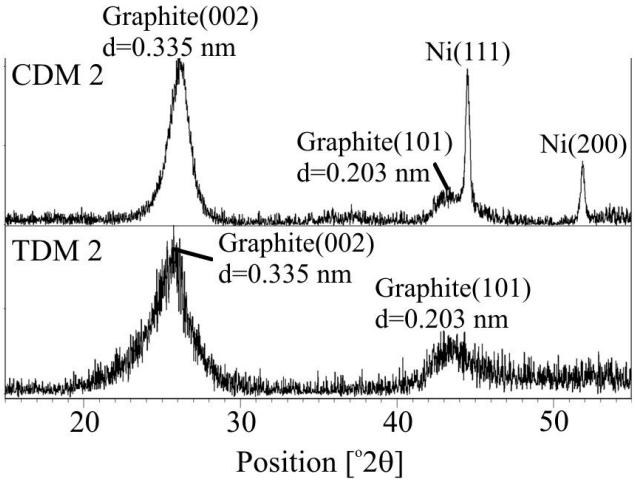

Figure 3. *The XRD patterns of the product carbons from CDM2 and TDM2.*

According to the literature (Kirk-Othmer, 2007), carbon black has a degenerated graphitic crystalline structure in 2D order whereas graphite has 3D order. Based on the XRD analyses, it is not possible to differentiate whether the structure of carbon from TDM 2 is 2D or 3D oriented. For comparison, in the study of Shah et al. (2001) the carbon produced by TDM at temperatures ranging between 900 °C and 1200 °C in a quartz reactor was stated as graphitic carbon.

3.3.2 SEM analyses

Product carbon from experimental runs TDM 2, CDM 2 and CDM 4 were selected for the SEM analysis.

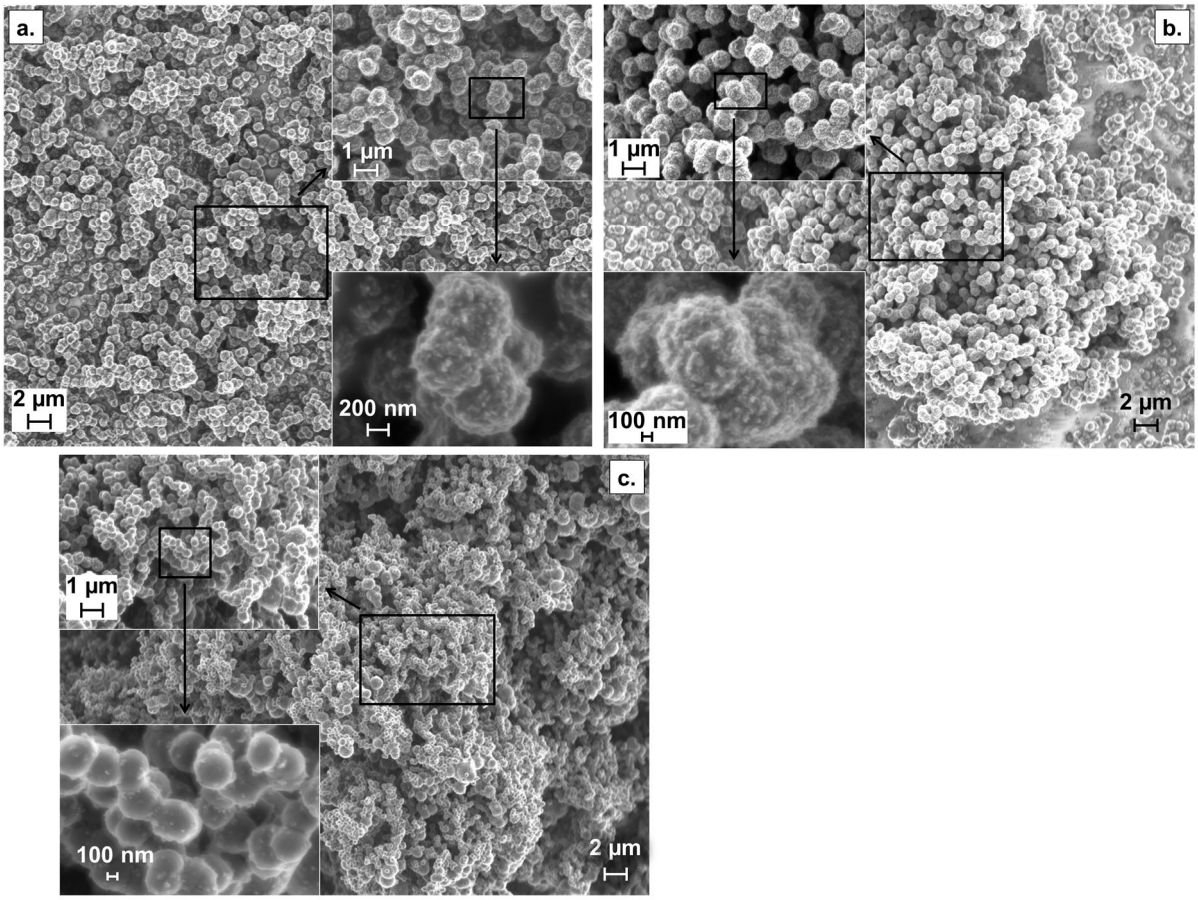

Figure 4. *The SEM images from three different spots of the product carbon TDM 2 with selected magnifications.*

The product carbon from TDM consisted of spherical carbon particles that had a diameter of less than 1 µ. The images presented in Fig. 4 show that the particles have formed aggregates and those have further agglomerated. The tendency to form aggregates rather than individual particles indicates a higher structure and better quality of the carbon black (Sebok and Taylor, 2011). Furthermore, variations in particle size and aggregate shape within a certain grade of carbon black are typical (Hess and Herd, 1993).

In this study, the size or surface roughness of the particles were not uniform in the studied sample but two different types could be discerned. First, there was an area where the carbon particles had a rather constant diameter and the particles had a coarse surface (Figs. 4a and b). Second, there was an area where the diameter of the particles varied, but the surface of the particles was smoother (Fig. 4c). The surface roughness may have an effect on the surface area of the carbon product.

Dahl et al. (2004) have produced carbon black via thermal decomposition of methane powered by concentrated sunlight. Their studies were conducted at temperatures up to 1860 °C and with short residence times. The product carbon was ash free and had a particle size of 20-40 nm (Dahl et al., 2004). According to the XRD-analysis, the product carbon was amorphous. Due to the small particles size, Dahl et al. were able to conduct TEM analyses for the product carbon. Their TEM images reveal the varying particle size distribution.

Particle size variation in the product carbon is also shown in the TEM images presented by Rodat et al. (2011), who have produced carbon black with TDM powered by concentrated solar radiations at a temperature range of 1335-1655 °C. They also compared the product carbon properties to those of commercial conductive carbon black. The result of the study by Rodat et al. was that the carbon produced at the highest temperature (1655 °C) had a structure and conductivity that were nearly consistent with the commercial carbon black.

The product carbons from runs CDM 2 and CDM 4 were selected to the SEM analysis because of the long period of methane conversion observed in these experiments. The SEM images of product carbon from run CDM 2 and CDM 4 are shown in Fig. 5.

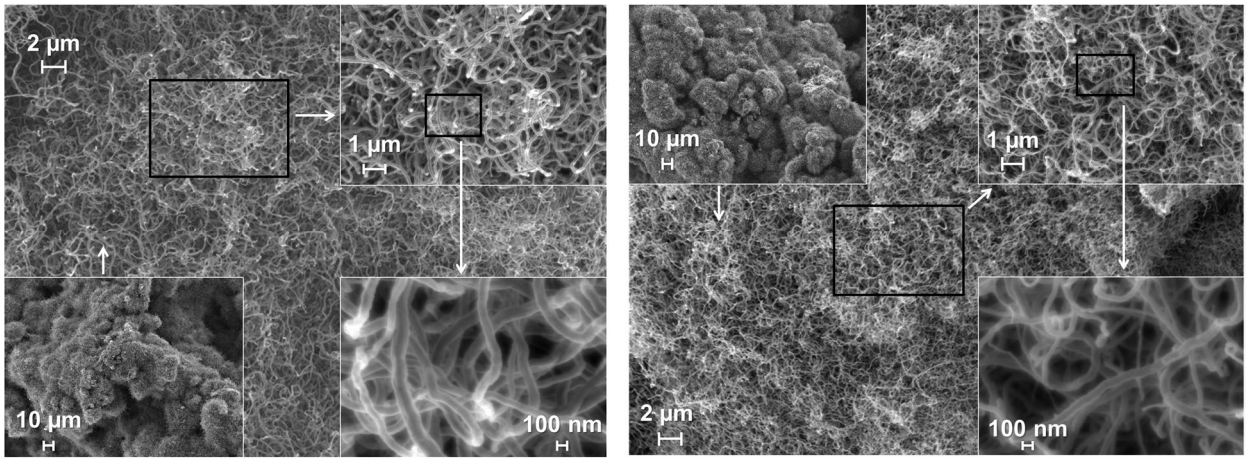

Figure 5. *The SEM images of the product carbon from CDM 2 (images on left) and from CDM 4 (images on right) with selected magnifications.*

The product carbon from the CDM experiments in this study was mainly filamentous carbon with a diameter varying mainly between 50-100 nm. It is worth noting that the length of a single carbon filament is high compared to the diameter.

The SEM images of the product carbon from CDM with nickel catalysts have been presented in CDM-related literature. Zhang et al. (2011 and 2010) have presented SEM images of carbon produced with non-supported nickel catalysts. The images in (Zhang et al., 2010) reveal how the carbon nanofibers have deposited themselves on the Ni catalysts. Another study by Zhang et al. (2011) presents SEM images of carbon nanofibers on the nickel catalyst. The carbon nanofibers were reported to have average diameters of 164 and 205 nm depending on the temperature during the CDM reaction.

3.3.3 TEM analyses

TEM images were taken from the product carbons resulting from runs CDM 2 and CDM 4 in order to better discover the structure of the carbon filaments in the samples. TEM images were not taken from TDM samples due to the too large carbon particle size.

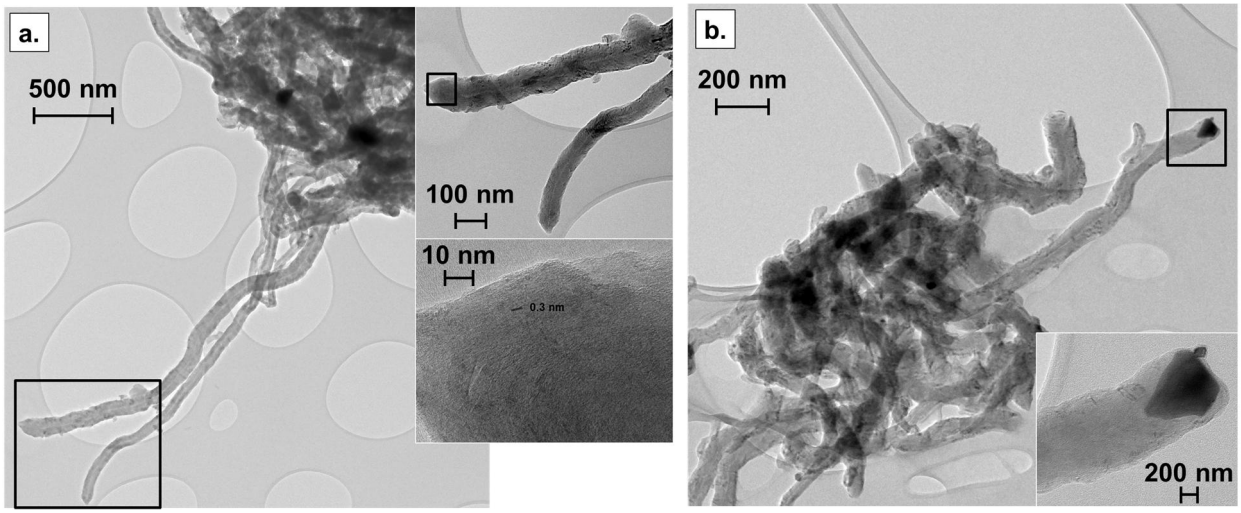

Figure 6. *The TEM images of product carbon from run CDM 2 with selected magnifications. The graphite platelets are separated by a distance of 0.3 nm, which is marked in the insert of the TEM image on the left.*

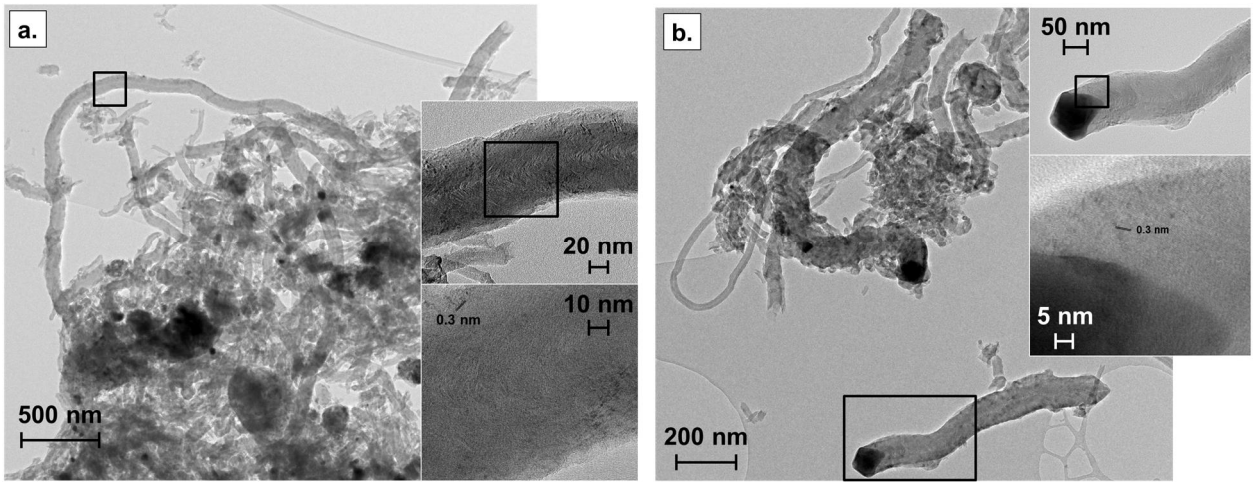

Figure 7. *The TEM images of the product carbon from run CDM 4 with selected magnifications. The graphite platelets are separated by a distance of 0.3 nm, which is marked in the inserts of the TEM images*.

As can be seen from Figs. 6 and 7 the diameter of the carbon fibers varies from tens to a few hundred nanometers. Moreover, the length of the fibers is high in comparison with the diameter of the fibers. Some of the carbon filaments in Fig. 7 are short and seem to be broken. A possible explanation for this is that the filaments have broken

during the sample preparation for the TEM analysis. An energy dispersive X-ray analysis (EDS) was conducted to find out the elementary composition of the darker spots in the TEM images. According to the EDS analyses, the particles at the tip of the filaments are nickel that originates from the catalyst. The diameter of the filament is roughly equal with the diameter of the catalyst particle, which agrees with the literature review presented in Section 2.2.

The TEM images with the highest magnification reveal that the selected carbon fibers have a herringbone structure. The observed spacing between the platelets was 0.3 nm (Figs. 6 and 7). The spacing between the platelets in graphite is 0.335 nm (Rodriguez et al., 1995).

Li et al. (2006) have presented TEM images of carbon produced by methane decomposition over a NiO catalyst. In the study of Li et al., the product carbon was in a form of nanofibers with Ni metal particles at their tips. Their nanofibers too have a herringbone structure, and the diameter of the nanofibers varied.

Lua and Wang (2013) have also presented TEM images of the product carbon from CDM with a nickel catalyst. In the study of Lua and Wang, methane decomposition with a Ni catalyst at 500 °C produced carbon fibers that have a diameter of 100 nm and Ni particles at their tips. Thus, the product carbon is highly similar to the carbon produced in this study. However, the diameter of the carbon fibers had a wider range in the study of Lua and Wang when the reaction temperature was increased to 550 °C. At that temperature, the product carbon consisted of carbon fibers with diameters of 10-50 nm as well as lumps of carbon fibers that covered nickel particles having a diameter of 100-200 nm. Wang and Lua (2014) had also presented TEM images of carbon nanofibers produced by CDM with an unsupported nickel catalyst. Variations in the diameter of the fibers are shown in these images.

4 Conclusion

The study of the thermo-catalytic decomposition of methane conducted at the Tampere University of Technology was continued by analyzing the product carbon samples obtained from experiments presented in Rajamäki (2014) and Keipi (2014). The X-ray diffraction, SEM and TEM analyses were conducted to the chosen product carbons from TDM and CDM experiments.

The product carbon from CDM experiments had a filamentous structure. The diameter of the carbon filaments varied from tens to a few hundred nanometers. There were nickel particles originating from the catalyst at the tip of carbon filaments. This referes to the tip growth mechanism of the carbon filaments during the methane decomposition reaction as presented in Section 2.2. Furthermore, the catalyst pellets broke down during the experimental runs, which supports this hypothesis.

The product carbon from TDM consisted of spherical particles with a diameter of less than 1 µm. The particles formed aggregates and finally agglomerates. The SEM images, which reveal the surface roughness, were also presented in this article. To the best of the author's knowledge, images revealing the same phenomenon have not been previously presented in studies related to methane decomposition. The surface roughness may have an effect on the physical properties of the product carbon, for example, on the specific surface area or electrical properties, and therefore on the utilization possibilities.

References

Publications at the Tampere University of Technology

M. Fager-Pintilä. 2012. Thermocatalytic decomposition of methane. Master´s Thesis, Tampere University of Technology, Finland.

M. Fager-Pintilä. 2013. Thermo-catalytic decomposition of methane: Annual report. Tampere University of Technology, Tampere. 44 p.

T. Keipi. 2014. Catalytic decomposition of methane – Experiments with metal catalysts, Tampere University of Technology, Tampere, 31 p.

T. Keipi, V. Hankalin, J. Nummelin, R. Raiko. 2016a. Techno-economic analysis of four concepts for thermal decomposition of methane: Reduction of CO_2 emissions in natural gas combustion. Energy Conversion and Management, 110:1-12. doi: 10.1016/j.enconman.2015.11.057

T. Keipi, K.E.S. Tolvanen, H. Tolvanen, J. Konttinen. 2016b. Thermo-catalytic decomposition of methane: The effect of reaction parameters on process design and the utilization possibilities of the produced carbon, Energy Conversion and Management 126:923-934. doi:10.1016/j.enconman.2016.08.060

M. Lappalainen. 2016. Comparison of two energy carriers and storage methods for renewable energy (Kahden uusiutuvan energian varastointimenetelmän ja energiankantajan vertailu), in Finnish. Tampere University of Technology, Bachelor's thesis.

J. Rajamäki. 2014. Thermal Decomposition and Autothermal Pyrolysis of Methane. Master of Science Thesis, Tampere University of Technology, Finland.

K. Tolvanen. 2013. Thermo-catalytic decomposition of methane – Carbon product utilization and market analysis. Tampere University of Technology, Tampere, 29 p.

Other references

H. F. Abbas, W. M. A. Wan Daud. 2010. Hydrogen production by methane decomposition: A review. International Journal of Hydrogen Energy, 35:1160-1190. doi:10.1016/j.ijhydene.2009.11.036.

A. M. Amin, E. Croiset, W. Epling. 2011. Review of methane catalytic cracking for hydrogen production. International Journal of Hydrogen Energy, 36:2904-2935. doi:10.1016/j.ijhydene.2010.11.035.

U. P. M. Ashik, W. M. A. Wan Daud, H. F. Abbas. 2015. Production of greenhouse gas free hydrogen by thermocatalytic decomposition of methane - A review. Renewable and Sustainable Energy Reviews, 44:221-256. doi:10.1016/j.rser.2014.12.025.

R. T. K. Baker. 2001. Encyclopedia of Materials: Science and Technology, Chapter: Carbon Nanofibers. Elsevier, pp. 932-941. doi:10.1016/B0-08-043152-6/00178-9.

T. D. Burchell. 2012. Comprehensive Nuclear Materials, Volume 2: Material Properties/Oxide Fuels for Light Water Reactors and Fast Neutron Reactors, Chapter: 2.10 - Graphite: Properties and Characteristics. Elsevier Ltd, pp. 285-305. doi:10.1016/B978-0-08-056033-5.00020-3.

J. K. Dahl, K. J. Buechler, A. W. Weimer, A. Lewandowski, C. Bingham. 2004. Solar-thermal dissociation of methane in a fluid-wall aerosol flow reactor, International Journal of Hydrogen Energy, 29:725-736. doi:10.1016/j.ijhydene.2003.08.009.

K. P. De Jong, J. W. Geus. 2000. Carbon Nanofiber: Catalytic Synthesis and Applications. Catalysis Reviews, 42:481-510.

E. Fitzer, K. Köhling, H. P. Boehm, H. Marsh. 1995. Recommended terminology for the description of carbon as a solid. Pure and Applied Chemistry, 67:473-506. doi:10.1351/pac199567030473.

M. J. Forest, Rubber Analysis - Polymer, Compounds and Products. 2001. Rapra Technology Ltd, technical report.

F. Frusteri, G. Italiano, C. Espro, C. Cannilla, G. Bonura. 2012. H_2 production by methane decomposition: Catalytic and technological aspects, International Journal of Hydrogen Energy, 37:16367-16374. doi:10.1016/j.ijhydene.2012.02.192.

P. J. F. Harris. 2009. Carbon Nanotube Science - Synthesis, Properties and Applications. Cambridge University Press, UK.

G. Heinrich, M. Klüppel. 2001. A hypothetical mechnanism of carbon black formation based on molecular ballistic deposition. Kautschuk und Gummi Kunststoffe, 54:159-165.

W. M. Hess and C. R. Herd. 1993. Carbon Black: Science and Technology, Marcel Dekker Inc., 1993, Ch. Microstructure, morphology and general physical properties, pp. 89–174.

International Energy Agency (IEA). 2015. Technology Roadmap: Hydrogen and fuel cells.

T. Keipi. 2014. Catalytic decomposition of methane – Experiments with metal catalysts, Tampere University of Technology, Tampere, 31 p.

T. Keipi, V. Hankalin, J. Nummelin, R. Raiko. 2016a. Techno-economic analysis of four concepts for thermal decomposition of methane: Reduction of CO_2 emissions in natural gas combustion. Energy Conversion and Management, 110:1-12. doi: 10.1016/j.enconman.2015.11.057.

T. Keipi, K.E.S. Tolvanen, H. Tolvanen, J. Konttinen. 2016b. Thermo-catalytic decomposition of methane: The effect of reaction parameters on process design and the utilization possibilities of the produced carbon, Energy Conversion and Management 126:923-934. doi:10.1016/j.enconman.2016.08.060

Kirk-Othmer (Ed.). 2007. Encyclopedia of Chemical Technology: Carbon Black. John Wiley & Sons Inc, New Jersey, USA.

J. Lahaye, G. Prado. 1974. Formation of carbon particles from a gas phase: nucleation phenomenon. Water, Air, & Soil Pollution, 3:473-481. doi:10.1007/BF00341000.

Y. Li, B. Zhang, X. Xie, J. Liu, Y. Xu, W. Shen. 2006. Novel Ni catalysts for methane decomposition to hydrogen and carbon nanofibers, Journal of Catalysis 238:412-424. doi:10.1016/j.jcat.2005.12.027.

Y. Li, D. Li, G. Wang. 2011. Methane decomposition to COx-free hydrogen and nanocarbon material on group 8-10 base metal catalysts: A review. Catalysis Today 162:1-48. doi:10.1016/j.cattod.2010.12.042.

A. C. Lua and H. Y. Wang. 2013. Decomposition of methane over unsupported porous nickel and alloy catalyst, Applied Catalysis B: Environment,132-133:469-478. doi:10.1016/j.apcatb.2012.12.014.

T. Morita, H. Inoue, Y. Suhara. 2002. US Patent US20020058139 A1.

N. Z. Muradov. 1998. CO_2-free production of hydrogen by catalytic pyrolysis of hydrocarbon fuel. Energy & Fuel, 12:41-48. doi:10.1021/ef9701145

R. L. Poveda, N. Gupta. 2016. Carbon Nanofiber Reinforced Polymer Composites, Chapter: Carbon Nanofibers: Structure and Fabrication. Springer International Publishing, pp. 11-26. doi:10.1007/978-3-319-23787-9.

J. Rajamäki. 2014. Thermal Decomposition and Autothermal Pyrolysis of Methane. Master of Science Thesis, Tampere University of Technology, Finland.

S. Rodat, S. Abanades, E. Grivei, G. Patrianakos, A. Zygogianni, A. Konstandopoulos, G. Flamant. 2011. Characterisation of carbon blacks produced by solar thermal dissociation of methane, Carbon 49:3084-3091. doi:10.1016/j.carbon.2011.03.030.

N. M. Rodriguez. 1993. A review of catalytically grown carbon nanofibers. Journal of-Materials Research, 8:3233-3250. doi:10.1557/JMR.1993.3233.

N. M. Rodriguez, A. Chambers, R. T. K. Baker. 1995. Catalytic engineering of carbon nanostructures. Langmuir, 11:3862-3866. doi:10.1021/la00010a042.

E. B. Sebok and R. L. Taylor. 2011. Encyclopedia of Materials: Science and Technology, Elsevier Ltd., Ch. Carbon Blacks, pp. 902-906. doi:10.1016/B0-750 08-043152-6/00173-X.

J. G. Speight. 2015. Handbook of Petroleum Product Analysis. John Wiley & Sons Inc, New Jersey, USA.

N. Triphob, S. Wongsakulphasatch, W. Kiatkittipong, T. Charinpantkul, P. Praserthdam, S. Assabumrungrat. 2012. Integrated methane decomposition and solid oxide fuel cell for efficient electrical power generation and carbon capture. Chemical Engineering Research and Design, 90:2223-2234. doi:10.1016/j.cherd.2012.05.014.

H. Y. Wang and A. C. Lua. 2014. Deactivation and kinetic studies of unsupported Ni and Ni-Co-Cu alloy catalysts used for hydrogen production by methane decomposition, Chemical Engineering Journal, 243:79-91. doi:10.1016/j.cej.2013.12.100.

W. Zhang, Q. Ge, H. Xu. 2010. Influences of precipitate rinsing solvents on Ni catalyst for methane decomposition to COx -free hydrogen, Journal of Physical Chemistry A, 114:3818-3823. doi:10.1021/jp906053h.

W. Zhang, Q. Ge, H. Xu. 2011. Influences of reaction conditions on methane decomposition over non-supported Ni-catalyst, Journal of Natural Gas Chemistry, 20:339-344. doi:10.1016/S1003-9953(10)60205-8.